

Development of magnetic domains in hard ferromagnetic thin films of polytwinned microstructure

A. Kazaryan and Y. Wang^{a)}

Department of Materials Science and Engineering, The Ohio State University, 2041 College Road, Columbus, Ohio 43210

Yongmei M. Jin, Yu U. Wang, and Armen G. Khachaturyan

Department of Ceramic and Materials Engineering, Rutgers University, 607 Taylor Road, Piscataway, New Jersey 08854

Lisha Wang and David E. Laughlin

Department of Materials Science and Engineering, Carnegie Mellon University, Pittsburgh, Pennsylvania 15213

(Received 26 June 2002; accepted 26 September 2002)

Three-dimensional computer simulations are used to examine the development of magnetic domains and migration of domain walls in hard ferromagnetic thin films of polytwinned microstructure. The polytwinned microstructure, consisting of three different orientation variants of the $L1_0$ ordered phase with orthogonal c -axes, is characterized by a multi-component long-range order (LRO) parameter. The coupling between the magnetic domains and the polytwinned microstructure is described by the coupling between magnetization and the LRO parameter in the anisotropy free energy of the system. The magnetodynamics is described by Landau–Lifshitz equations that are solved numerically in the reciprocal space using a parallel Fast Fourier Transform algorithm. It is found that the coupling results in a multilevel hierarchy in the magnetic domain structure, with intracolony boundaries (across multiple variants within a single polytwinned colony) and intercolony boundaries (across multiple colonies). In thin films of high magnetic anisotropy we find the intracolony boundary to be of $\{100\}$ type and the intercolony one to be on average of $\{110\}$ type. The migration of the magnetic domain boundaries in external magnetic fields is studied in a number of simple cases in which the fields are applied along different directions. The simulation results are analyzed and compared with existing experimental observations. © 2002 American Institute of Physics. [DOI: 10.1063/1.1522494]

I. INTRODUCTION

The miniaturization of electronic devices demands higher and higher density of magnetic recording media. As the density of magnetic storage increases, the grain size of the magnetic materials used to store the information must also decrease to keep the signal-to-noise ratio acceptable. However, as the grain size decreases, the materials approach what is known as the superparamagnetic limit.¹ To counteract this, materials with high magnetocrystalline anisotropy must be utilized. Of particular interest in this regard are high anisotropy materials such as CoPt and FePt.^{1,2} At room temperature, these alloys have an $L1_0$ ordered structure that is an fcc derivative structure with tetragonal symmetry. In these materials, there are structural domains (orientation variants), translational domains (antiphase domains), and magnetic domains. The c -axis of the tetragonal orientation variant coincides with the easy magnetization axis. The interplay between the development of these features dominates the magnetic properties of these materials and, therefore, it is desirable to understand and predict how these features are coupled with each other.

Analytically magnetic domain structure can be predicted only in a limited number of simplified cases, typically in plates or ellipsoids with uniaxial magnetic anisotropy.^{3,4} In materials with more complicated underlying atomic microstructures, analytical solutions for their magnetic domain structures are usually unattainable. Furthermore, experimental studies have serious difficulty in providing the details of the coupling between the structural and magnetic domains and the corresponding effect on the development of the magnetic domain structures. In this article we employ computer simulations to explore this coupling effect. Of particular interest are the multilevel hierarchy in the magnetic domain structure, the orientations of the magnetic domain boundaries, and their migration in an applied magnetic field.

Micromagnetic modeling has been used extensively to study magnetization process in soft and hard magnetic materials. A number of computer simulation models have been developed to characterize correlations between the magnetic domains and the underlying microstructure in various materials systems. Among them, the most popular and successful ones are: (a) the adaptive finite element micromagnetic approach^{5–8} and (b) the approach by Bertram and Zhu,^{9–11} who solved the Landau–Lifshitz equations in the reciprocal space using the Fast Fourier Transform (FFT) technique. The former method has been used extensively in the development

^{a)} Author to whom correspondence should be addressed; electronic mail: wang.363@osu.edu

and optimization of high-performance permanent magnets, advanced magnetic recording media, and magnetic sensors, while the latter has been used widely in modeling magnetic properties of thin film granular media in which each grain is treated as a uniformly magnetized domain and represented by a single point on the computational mesh.

Similar to the latter approach, in this study we solve the Landau–Lifshitz equations for a single crystal of polytwinned domain structure in the reciprocal space using FFT. The three different orientation variants of the $L1_0$ phase in the polytwinned structure are described by a multicomponent long-range order (LRO) parameter. The coupling of the magnetic domains to the polytwinned domains is described through the coupling between the magnetization and the LRO parameter in the anisotropy free energy of the system. One of the major advantages of using this approach is that it is fully compatible with the well-developed phase field method for complex structural domain formation in various materials systems.^{12–18} It allows for a straightforward and self-consistent consideration of the interactions between the structural and magnetic domains, and their interactions with external fields (stress and magnetic). These interactions may alter dramatically the time evolution of both the structure and magnetic domains and hence provide a variety of opportunities to tailor the structure-sensitive properties through thermal mechanical processing under applied magnetic and stress fields. This appears to be especially important for the consideration of magnetostriction and for the study of systems in which the structural transition temperature is close to or lower than the Curie temperature (such as magnetic shape memory alloys). It will also allow for the consideration of various magnetic defects associated with crystalline defects such as imperfect grain boundaries and domain boundaries, second-phase particles, and dislocations.

The foci of the current study are on the hierarchy of the magnetic domain structures, the orientations of the magnetic domain boundaries, and their migration in the presence of externally applied magnetic fields in thin films of hard magnetic materials with a fixed polytwinned microstructure. Experimental studies of the magnetic domain structure in polytwinned crystals^{19–21} have identified the cooperative nature and multilevel hierarchy of the magnetic domains with the formation of *micro-* (coinciding with individual orientation variants) and *macro-* (containing multiple structural variants) domains. However, the existing results disagree with each other on the fundamental issue of the orientation of the boundaries between the macrodomains, which plays the dominant role in the magnetization reversal process and, therefore determines the hysteretic properties of these materials. We first introduce the model and materials parameters employed in the computer simulations, followed by description and discussion of the simulation results. The same approach has also been applied to study the effect of grain boundaries and grain texturing in a polycrystalline hard magnetic thin film on the magnetic properties.²²

II. MICROMAGNETIC MODEL

According to the phenomenological theory used in micromagnetics, the temporal evolution of the ferromagnetic

domains of a system is described by the damping term of the time-dependent Landau–Lifshitz equations:²³

$$\frac{\partial \mathbf{M}(\mathbf{r}, t)}{\partial t} = -\frac{\lambda}{M_s} [\mathbf{M}(\mathbf{r}) \times (\mathbf{M}(\mathbf{r}) \times \mathbf{H}_{\text{eff}}(\mathbf{r}))] \quad (1)$$

where $\mathbf{M}(\mathbf{r})$ is the magnetization vector, M_s is the value of saturation magnetization, $\mathbf{H}_{\text{eff}}(\mathbf{r})$ is the net magnetic field at the point \mathbf{r} created by all the internal and external sources, and λ is a positive constant that characterizes the damping of magnetization. In general, the effective field, $\mathbf{H}_{\text{eff}}(\mathbf{r})$, acting on the magnetic moment of a unit volume can be represented as a variational derivative of the total energy of the system with respect to magnetization:

$$\mathbf{H}_{\text{eff}}(\mathbf{r}) = -\delta E / \delta \mathbf{M}(\mathbf{r}). \quad (2)$$

The total energy of a ferromagnetic system with an arbitrary magnetization distribution $\mathbf{M}(\mathbf{r})$ is given by

$$E = E_{\text{anis}} + E_{\text{exch}} + E_{\text{ms}} + E_{\text{app}}, \quad (3)$$

where E_{anis} is the anisotropy energy, E_{exch} is the exchange energy, E_{ms} is the magnetostatic interaction energy, and E_{app} is the energy due to externally applied magnetic fields. Next we give a brief description for each of these terms.

A. Anisotropy energy

In this article we consider a polytwinned microstructure consisting of three orientation variants of an $L1_0$ ordered phase of tetragonal symmetry. The tetragonality axes (c -axes) of the variants are along the three cubic directions ($[100]$, $[010]$, and $[001]$) of the disordered cubic parent phase, and they are also the easy magnetization axes (anisotropy axes). Therefore, each of the orientation variants can be viewed as a uniaxial single crystal with its c -axis being the anisotropy axis. The anisotropy energy of a crystal with uniaxial magnetic symmetry is given by

$$E_{\text{anis}} = \int \{K_1 \sin^2[\theta(\mathbf{r})] + K_2 \sin^4[\theta(\mathbf{r})]\} d^3r, \quad (4)$$

where $\theta(\mathbf{r})$ is the angle between the magnetization vector and the anisotropy axis of the crystal and K_1 and K_2 are the anisotropy constants.

In the phase field approach, the three orientation variants of the $L1_0$ ordered phase are described by three field variables $[\eta_i(\mathbf{r})$ ($i=1,2,3$), called the LRO parameter] that characterize the $L1_0$ ordering. $\eta_i(\mathbf{r})$ can be viewed as a shape function of the i th orientation variant, with its value equal to unity inside the i th orientation variant and zero elsewhere. Using (η_1, η_2, η_3) to describe the distribution of the easy magnetization axes, and considering the fact that $K_1 \gg K_2$ in the material systems that we are interested in, we can rewrite Eq. (4) in the following form:

$$E_{\text{anis}} = \int K_1 [1 - (m_x^2 \eta_1^2 + m_y^2 \eta_2^2 + m_z^2 \eta_3^2)] d^3r, \quad (5)$$

where m_i are the components of the unit magnetization vector, $\mathbf{m} = \mathbf{M} / M_s$.

B. Exchange energy

The magnetic moments in a ferromagnet are coupled by a short-range exchange interaction. In this article we assume that all structural boundaries are “perfect,” that is, the magnetization vector $\mathbf{M}(\mathbf{r})$ has a constant absolute value throughout the system and the exchange energy across the structural boundaries are the same as in the bulk. In this case the exchange energy is determined solely by the spatial variation of the magnetization orientation and can be written as:

$$E_{\text{exch}} = \int \frac{\beta}{2} (\nabla_i m_j) (\nabla_i m_j) d^3 r, \quad (6)$$

where β is a positive constant.

C. Magnetostatic energy

In contrast to all these contributions to the system energy, which are the local terms, the magnetostatic energy is highly nonlocal. The total magnetostatic energy of a system with an arbitrary ferromagnetic domain structure can be written as:⁴

$$E_{\text{ms}} = -2\pi M_s^2 \int (\mathbf{m}(\mathbf{r}) \cdot \mathbf{h}_d(\mathbf{r})) d^3 r, \quad (7)$$

where $\mathbf{h}_d(\mathbf{r})$ is the demagnetization field that is determined by the long-range interaction among the magnetic moments in the system. Several methods have been suggested in the literature to calculate $\mathbf{h}_d(\mathbf{r})$, which can be grouped into two major categories.²⁴ The first one is to solve the Maxwell's equations using the concept of magnetostatic potential (scalar or vector). Another approach is to use the dipolar approximation

$$\mathbf{h}_d(\mathbf{r}) = \int \frac{3\mathbf{e}[\mathbf{m}(\mathbf{r}') \cdot \mathbf{e}] - \mathbf{m}(\mathbf{r}')}{|\mathbf{r} - \mathbf{r}'|^3} d^3 r', \quad (8)$$

where \mathbf{e} is a unit vector along $(\mathbf{r} - \mathbf{r}')$. The latter is employed in the current study. For numerical simulations, calculation of the magnetostatic energy is the most time consuming part, since it involves double integrals and, therefore, scales as $O(N^2)$ (where N is the system size, that is, the number of mesh points on the computational grid). To overcome this difficulty, we utilize the FFT technique that has been successfully applied for the calculation of elastic energies in systems containing dislocations, coherent precipitates, etc., which from the mathematical point of view is very similar to the calculation of magnetostatic energies.²⁵ The advantage of this technique is that the number of computational operations scales as $N \log(N)$ instead of N^2 . Substituting Eq. (7) into Eq. (6) and making use of the Fourier representations, E_{ms} can be written as²⁴

$$E_{\text{ms}} = 2\pi M_s^2 \int \frac{d^3 k}{(2\pi)^3} |\mathbf{n}\{\mathbf{m}(\mathbf{r})\}_{\mathbf{k}}|^2, \quad (9)$$

where $\mathbf{n} = \mathbf{k}/|\mathbf{k}|$ is a unit vector in the reciprocal space and $\{\dots\}_{\mathbf{k}}$ denotes the Fourier transform. Note that $\mathbf{k} = 0$ is a singularity point and is excluded from the integration. It should be noted that FFT technique has been used previously in a number of studies, where the concept of magnetostatic potential was used to calculate the demagnetization field.²⁴

D. Energy due to external field

The effect of an externally applied magnetic field \mathbf{H}_{ext} on the system energy can be taken into account through the interaction between the magnetization and the external field:

$$E_{\text{app}} = -M_s^2 \int (\mathbf{h}_{\text{ext}} \cdot \mathbf{m}) d^3 r, \quad (10)$$

where $\mathbf{h}_{\text{ext}} = \mathbf{H}_{\text{ext}}/M_s$. It should be noted that when the external field is uniform, this energy depends only on the average value of magnetization and is independent of the specific domain structure or the shape of the system.

Substituting Eqs. (5), (6), (9), and (10) into Eq. (2), we have

$$(H_{\text{eff}})_i = -\frac{\delta E}{\delta M_i} = \frac{2K_1}{M_s} m_i \eta_i^2 + \frac{\beta}{M_s} \Delta m_i - 4\pi M_s \{(\mathbf{n} \cdot \{\mathbf{m}\}_{\mathbf{k}}) n_i\}_{\mathbf{r}} + (\mathbf{H}_{\text{ext}})_i. \quad (11)$$

For the convenience of numerical solutions we rewrite Eq. (1) in its dimensionless form:

$$\frac{\partial \mathbf{m}(\mathbf{r}, t)}{\partial \tau} = -[\mathbf{m}(\mathbf{r}) \times (\mathbf{m}(\mathbf{r}) \times \mathbf{h}_{\text{eff}}(\mathbf{r}))], \quad (12)$$

which is obtained by dividing both sides of Eq. (1) by $2\pi\lambda M_s^2$. In Eq. (12), $\tau = 2\pi\lambda M_s^2 t$ is the reduced time, t is time and $\mathbf{h}_{\text{eff}} = \mathbf{H}_{\text{eff}}/2\pi M_s$. Length scale of the simulation is now measured in the units of reduced length $\rho = r/l_0$, where l_0 is the grid size. The computer simulations are performed on a cubic lattice with $\Delta\rho = 1$ and $\Delta\tau = 0.005$.

III. RESULTS AND DISCUSSION

The solution of Eq. (12) has been used to study the effect of coupling between the magnetic and structural domains in hard ferromagnetic thin films. The schematic drawing of a polytwinned structure consisting of three orientation variants is presented in Fig. 1. It can be readily seen that the polytwinned structure has a complex multilevel hierarchy of the structural features, with the basic building blocks being the three individual orientation variants (the C-domains) of the tetragonal phase. The letters “X,” “Y” and “Z” denote the tetragonality axis of the variants. The tetragonality axis is the easy magnetization axis; that is, each C-domain is a magnetically uniaxial crystal with the easy axis along X-, Y-, or Z-directions. During the structural transformation, the orientation variants arrange themselves into polytwinned plates of $\{110\}$ habits (thick solid lines in Fig. 1) to minimize the elastic energy. These polytwinned plates are often referred to as *colonies* with each colony consisting of only two types of the orientation variants (e.g., X and Z or Y and Z in Fig. 1). Finally, a polytwinned microstructure may contain many colonies of different habit plane orientations that are arranged into *packets* (not shown in Fig. 1), representing the highest level of microstructural hierarchy in a polytwinned structure. We adopt the following notation: d - characteristic size of individual orientation variant, L_c - characteristic colony size, and L_p - characteristic packet size.

The model system considered in this study is a laterally infinite thin film of thickness δ . Computer simulations have

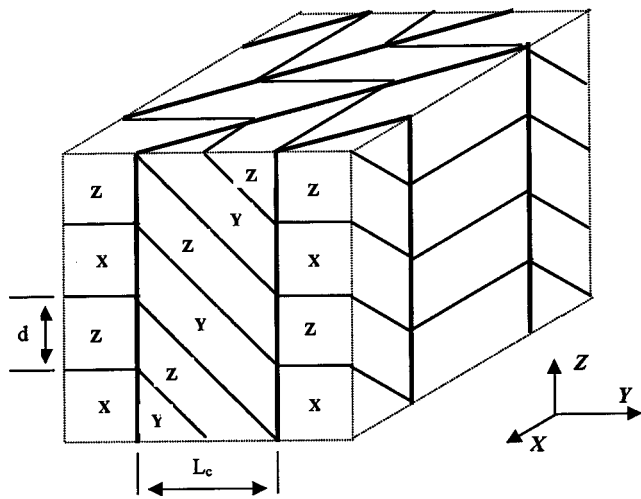


FIG. 1. Schematic drawing of a single packet of a polytwinned microstructure. The structure is periodically repeated in the X–Y directions. Thin solid lines—twin boundaries; thick solid lines—boundaries between the colonies of twins. Labels X, Y, and Z denote the tetragonality axis of the individual orientation variants. d is the characteristic thickness of an orientation variant and L_c is the characteristic size of the colony.

been performed on a $128 \times 128 \times 128$ cubic mesh, where the film has a thickness of 32 grid points (along the Z-direction) and the rest is left as empty space (vacuum). Periodic boundary conditions are imposed along all three dimensions. The selection of 96 grid points in vacuum and 32 grid points in the sample along the Z-direction is to avoid possible overlaps of the stray fields from neighboring computational cells introduced by the periodical boundary conditions. The typical penetration length of the stray field into vacuum is of the order of average magnetic domain size near the surface, which is of the order of 32 grid points. Therefore, the chosen space in vacuum between two computational cells is considerably larger than the penetration length of the stray field.

The following values of the dimensionless parameters have been used in the computer simulations: $K^* = K/2\pi M_s^2 = 7.96$, $\beta^* = \beta/2\pi M_s^2 l_0^2 = 6.0$. These parameters correspond to the FePt system.¹⁹ In order to determine the length scale of the simulation, which is defined by the scale of the computational grid increment l_0 , we compare the experimentally observed value of the magnetic domain wall energy density for the 180° Bloch wall, γ_{exp} , with the one that is calculated from our computer simulation, γ^* . The two are related with each other as $\gamma_{\text{exp}} = \gamma^* l_0^2 / 2\pi M_s^2$. Using $\gamma^* = 23.9$ and $\gamma_{\text{exp}} / 2\pi M_s^2 = 4 \times 10^{-7}$ m (which corresponds to the FePt system¹⁹), the length scale of the simulation is $l_0 = 2.6$ nm.

The computer simulation results are presented in Fig. 2, which shows the three components of the magnetization field by different shades of gray, with the brightest corresponding to the value of +1, darkest to minus -1, and shades in between representing intermediate values. The nine pictures for each magnetization component correspond to nine consecutive slices along the Z-direction (001), which is the plane of observation. The simulations are started from a state in which each point has a random orientation of the magnetization field. The magnetic state of the system shown in Fig. 2 corresponds to reduced time $\tau = 1000$. Figure 3 presents

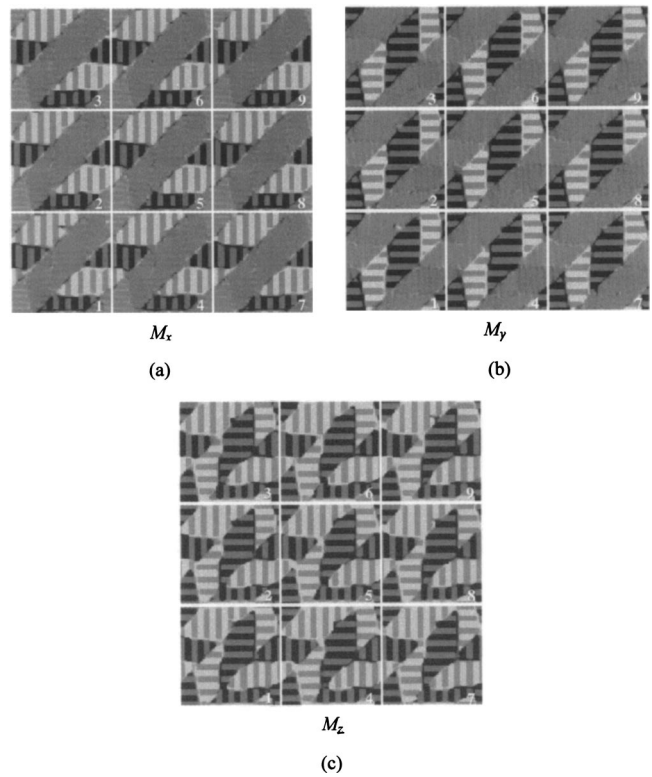


FIG. 2. Simulated magnetic domains in a thin film of hard ferromagnetic material with polytwinned microstructure. The plane of observation is (001). The following color scheme has been adopted in the above figures: white color represents value of +1, black a value of -1 and different shades of gray are the intermediate values. The nine pictures for each of the magnetization components correspond to different slices along the Z-direction (film thickness).

schematic drawing of the magnetic domain structures, and the corresponding magnetization field on (001) and (010) planes of the film that corresponds to our simulation results presented in Fig. 2. Examining the three components of the magnetization vector shown in Figs. 2 and 3, one can see that the magnetization in each orientation variant is directed along its tetragonality axis (is associated with only one magnetic component). For example, the variants with their c -axis along the X-direction have $\mathbf{M} = M_s (\pm 1, 0, 0)$ [shown as domains of bright and dark shades in Fig. 2(a)]. This magnetization alignment is the result of minimizing the anisotropy energy that is extremely high in FePt alloys. Below we refer to such a level of hierarchy in the magnetic domain structure (e.g., at the scale of individual variant) as *microdomains*. These predictions agree well with the experimental observation.²¹

The next level of hierarchy of the magnetic domain structure is observed at the scale of twin plates or colonies consisting of two twin-related variants. It can be seen from Fig. 2 that within each colony of uniform twin structure there exist multiple magnetic domains. Across the domain boundaries the magnetization components change their sign. In Fig. 2(a), for example, $\mathbf{M} = M_s (1, 0, 0)$ (bright) on one side of the boundary and changes to $\mathbf{M} = -M_s (-1, 0, 0)$ (dark) on the other side of the boundary. The same is true for M_y and M_z [Figs. 2(b) and 2(c)]. We call the magnetic domain boundary that crosses multiple orientation variants within a

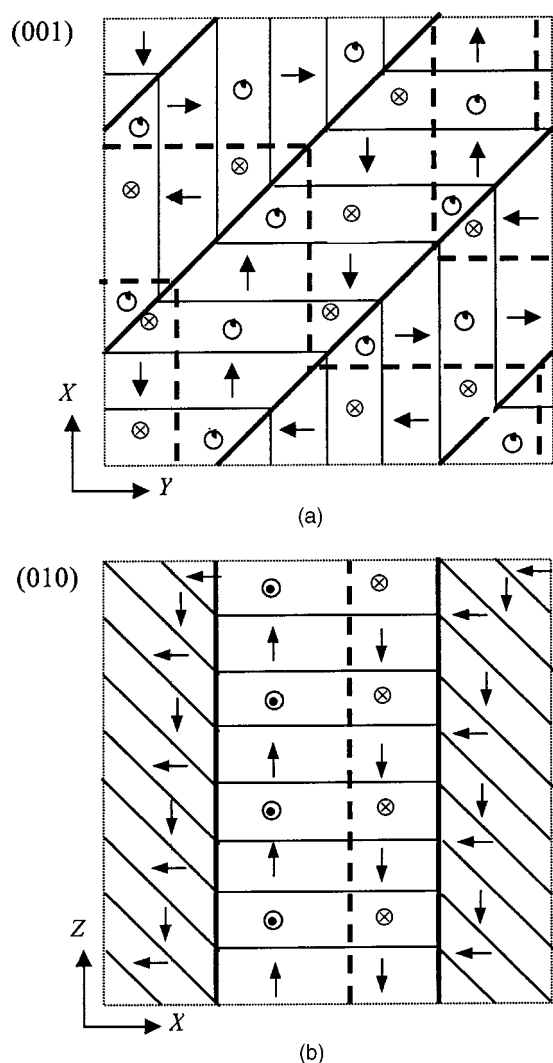


FIG. 3. Schematic drawings of the magnetic domains with $\{100\}$ type of macrodomain boundary. The two cross sections that are shown correspond to (a) (001) plane and (b) (010) plane. The underlying microstructure is presented as follows: thin solid lines—twin boundaries; thick solid lines—boundaries between colonies. Thick dashed lines correspond to the intradomain boundaries. Orientation of magnetization in each structural orientation variant is shown by the arrows.

colony an *intra*colony boundary. One can also see that these intracolony boundaries have either (100) or (010) orientation depending on the colony (see the dashed lines on the schematic drawing in Fig. 3). Finally, the intracolony boundaries in the neighboring colonies are interconnected with each other and form a continuous boundary wiggling through the entire packet. We call this boundary the *intercolony* boundary. On average, the intercolony boundary has a $\{110\}$ type orientation (Fig. 3).

Experimental investigations of magnetic domain structure suggest that the intercolony boundary can be of either $\{110\}$ or $\{111\}$ type.^{19–21} In particular, observations of the magnetic domain structures on both (001) and (011) surfaces by Vlasova *et al.*¹⁹ lead to a conclusion that the intracolony boundaries have an $\{110\}$ type orientation and the intercolony boundaries have an $\{111\}$ type orientation. On the other hand, observations by Zhang and Soffa²⁰ and Wang, Fan, and Laughlin²¹ suggest that the intercolony boundaries

have a $\{110\}$ type orientation. Later, we analyze the formation and evolution of the magnetic domain structure from the point of view of “magnetostatic charges,” with particular emphasis on the orientation of the magnetic domain boundaries and their migration under external magnetic fields. Although there is a wide range of possibilities for the spatial orientation of the intercolony domain boundaries, we examine the ones that have $\{110\}$ or $\{111\}$ orientations, since they are the ones that have been observed in the experimental studies.

Formation of such a multilevel hierarchy of the magnetic domain structure is not surprising, and can be explained by the requirement of the absence of magnetostatic charges. Analyzing the schematic drawings in Fig. 3, one can see that if a magnetic domain boundary runs across individual variants, it should be oriented perpendicularly to the boundaries between the two twin-related variants to avoid magnetostatic charges at the boundaries. For the same reason, the intercolony boundaries have to be continuous across the structural boundary between two colonies. As a consequence, the orientations of both the intra- and intercolony boundaries are determined by the condition that no magnetostatic charges are created, leading to a multilevel hierarchy magnetic domain structure.

Another possible way to arrange the magnetic domains into the multilevel hierarchy structure without creating magnetostatic charges is illustrated schematically in Fig. 4. It shows the magnetic domain structure in the (001) and (100) planes of such a configuration, in which the intracolony boundary has on average a $\{110\}$ type orientation [Fig. 4(b)] and the intercolony domain boundary has a $\{111\}$ type orientation. However, in contrast to the previous case, the $\{110\}$ type intracolony boundary has a twice-larger area (due to the zigzag nature of this boundary). If we assume that the specific energy of the intracolony boundaries is the same for the two types of boundaries, the boundaries of the $\{110\}$ orientations would have twice as much energy as those of the $\{100\}$ orientations. However, the boundary type that is preferred by the system is the one that minimizes the total energy (in our case this will be the sum of the magnetostatic energy and domain boundary energy) rather than the boundary energy alone. To determine the energetics of the two types of boundaries, we calculate the total system energy for each case numerically using Eqs. (5), (6), and (9). It is found that the $\{110\}$ type intercolony boundary is indeed energetically favorable. The result appears to be unchanged for different thickness of the orientation variant, different colony size and film thickness. In particular, each of these parameters has a fourfold variation in the calculations and in all the cases the $\{110\}$ type boundary has lower total energy. This explains why only one type of boundary is observed in the computer simulations.

Finally, using the computer simulation we have studied the effect of externally applied magnetic fields on the migration of the intra- and intercolony boundaries. First, the field is applied in the direction of $(1, -1, 0)$. This is the simplest case since the structural boundary between the neighboring colonies is also a magnetic domain boundary where the domains with $m_x = +1$ and $m_y = -1$ (and vice versa) contact

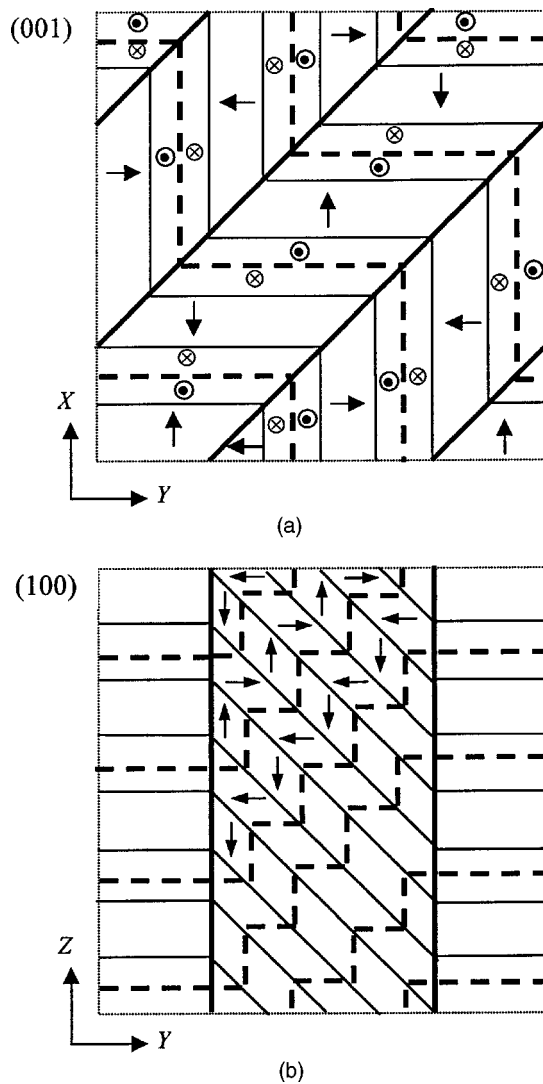


FIG. 4. The same as in Fig. 3 but with {110} type of intradomain boundary.

each other (see Fig. 3). Since the applied field has equal components along the m_x and $-m_y$ directions, both domains are favored equally over the others. As a consequence, these domains should expand at the expense of the others. However, within the colonies where either X- or Y-variants present, only 50% of the variants are the X- or Y-variants (the rest are the Z-variants). One would expect that only the intracolony boundaries within these variants to migrate in correspondence to the external field. However, what we found in the simulation is that the boundary migrates as a whole across the entire colony [see the solid lines in Figs. 5(a) and 5(b)]. Moreover, the intracolony boundaries within different colonies migrate at the same velocity (because boundary segments in different colonies are favored equally by the applied field) and consequently the entire intercolony boundary migrates as a whole as well [see Fig. 5(b)].

Next, a field is applied along the X-direction. In this case, the orientation variants with the easy axis along the X-direction are present only in the alternating colonies. The migration of the intercolony boundary is expected to occur only in these colonies where the X-variants are present. What we find in the simulation is that the entire intercolony

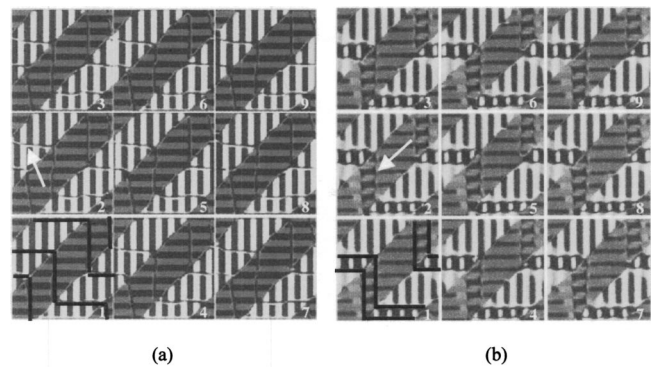


FIG. 5. Simulated magnetic domain structure in a system with (a) $\mathbf{h}_{\text{ext}}=0$ and (b) $\mathbf{h}_{\text{ext}}=(0.5,-0.5,0)$. The shades of gray in the micrographs correspond to the values of $|m_x|-|m_y|-2|m_z|$, from dark (-2) to bright (+1). The nine pictures in each micrograph correspond to nine consecutive slices along the (001) direction. Magnetic domain boundaries can be seen as continuous lines, as indicated by the arrows and outlined by solid black lines at the bottom-left corners.

boundary migrates as a whole under the influence of the external field. This result is the same as what is obtained in the previous case, with the only difference being the much slower migration velocity of the boundary. The reason for such a collective boundary motion is that the intercolony domain boundary has to be continuous across the boundary between two colonies to avoid magnetostatic charges. When the external field is applied along the Y-direction, similar results are obtained. Therefore, the collective motion of both the intra- and intercolony boundaries observed in the computer simulations is a direct consequence of the requirement of the absence of magnetostatic charges at the boundaries between the individual orientation variants and the boundaries between the colonies.

When a magnetic field is applied along the Z-direction, however, very different domain wall motion is expected because both neighboring colonies contain Z-variants that have opposite magnetization; i.e., if the first colony has a variant with $m_z=+1$, its neighbor in the second colony will have $m_z=-1$. In the presence of an external field applied along the Z-direction, domains containing $+m_z$ will grow and domains containing $-m_z$ will shrink. However, this will create a discontinuity in the intercolony boundaries and result in magnetostatic charges at the boundary between the structural colonies and therefore should be prohibited. In a more general case, in which the magnetic field is applied in an arbitrary direction, the response of the system can be quite complicated, and the problem is under investigation.

Another interesting application of the model is to study the coupled evolution of structural and magnetic domains in ferromagnetic shape memory alloys with high magnetostriction. In these materials the martensitic transition temperature is comparable or lower than the Curie temperature. Of particular interest is to examine how an applied magnetic or stress field modifies the structural and magnetic domains and their magnetic properties. Corresponding work is under way.

IV. CONCLUSIONS

A micromagnetic approach has been used to study the effects of coupling between the magnetic domains and the

underlying microstructure on magnetic domain development and domain wall migration in ferromagnetic thin films. In particular, the model is applied to examine the formation of magnetic domains in hard ferromagnetic thin films (50–100 nm) such as FePt alloys with polytwinned microstructures. From the computer simulations, it is found that magnetic domains form a collective hierarchical structure consisting of micro- (at the scale of individual variants) and macrodomains (at the scale of internally twinned colonies) with intra- and intercolony boundaries. The intracolony boundaries have either (100) or (010) orientation perpendicular to the boundary between two twin-related variants, while the intercolony boundaries have on average {110} orientation. This is in contrast to the previous experimental studies that conclude that in bulk FePt intercolony boundaries have on average {111} orientation. The results are confirmed by direct energy calculations, which show that in thin films intercolony boundaries with {110} orientation are indeed energetically favorable as compared to {111} oriented boundaries. In addition, the micromagnetic model is applied to study the migration of the magnetic domain boundaries in the presence of externally applied magnetic fields. It is found that the entire domain boundary migrates as a whole to preserve the continuity of the intra- and intercolony boundaries and to avoid magnetostatic charges. This behavior should play an important role in the remagnetization process.

ACKNOWLEDGMENTS

We gratefully acknowledge the financial support of NSF under grant DMR-9905725. Computer simulations were performed at San Diego Supercomputer Center.

¹D. Weller *et al.*, IEEE Trans. Magn. **36**, 10 (2000).

- ²J. A. Christodoulides *et al.*, J. Appl. Phys. **87**, 6938 (2000).
³L. D. Landau and E. M. Lifshitz, *Electrodynamics of Continuous Media* (Oxford, Oxford, 1960).
⁴A. Hubert and R. Schafer, *Magnetic Domains. The Analysis of Magnetic Microstructures* (Springer, Berlin, 1998).
⁵for a recent review see T. Schrefl, J. Magn. Magn. Mater. **207**, 45 (1999).
⁶T. Schrefl and J. Fidler, J. Magn. Magn. Mater. **177–181**, 970 (1998).
⁷R. Fischer and H. Kronmüller, Phys. Rev. B **54**, 7284 (1996).
⁸J. C. Lodder, J. Magn. Magn. Mater. **159**, 238 (1996).
⁹H. N. Bertram and J.-G. Zhu, Solid State Phys. (edited by H. Ehrenreich and D. Turnbull), **46**, 271 (1992).
¹⁰J.-G. Zhu, in *Magnetic Recording Technology* (edited by C. D. Mee and E. D. Daniel) (McGraw-Hill, New York, 1996).
¹¹J.-G. Zhu, *Magnetic Imaging and Its Applications to Materials*, Experimental Methods in The Physical Sciences Vol. 36, edited by M. D. Graef and Y. Zhu (Academic, New York, 2001).
¹²for recent reviews see Y. Wang and L.-Q. Chen, in *Methods in Materials Research* (Wiley, New York, 1999); L.-Q. Chen and Y. Wang, JOM **48**, 13 (1996).
¹³A. Karma and W.-J. Rappel, Phys. Rev. E **57**, 4323 (1998).
¹⁴A. Kazaryan, Y. Wang, S. A. Dregia, and B. R. Patton, Phys. Rev. B **61**, 14275 (2000); *ibid.* **63**, 184102 (2001).
¹⁵Y. U. Wang, Y. M. Jin, A. M. Cuitino, and A. G. Khachatryan, Acta Mater. **49**, 1847 (2001).
¹⁶Y. U. Wang, Y. M. Jin, and A. G. Khachatryan, J. Appl. Phys. **91**, 6435 (2002).
¹⁷S. Semenovskaya and A. G. Khachatryan, J. Appl. Phys. **83**, 5125 (1998).
¹⁸Y. L. Li, S. Y. Hu, Z. K. Liu, and L.-Q. Chen, Acta Mater. **50**, 395 (2002).
¹⁹For a recent review see N. I. Vlasova, G. S. Kandaurova, and N. N. Schegoleva, Phys. Met. Metallogr. **90**, 239 (2000).
²⁰B. Zhang and W. A. Soffa, Phys. Status Solidi A **131**, 707 (1992); B. Zhang and W. A. Soffa, Scr. Mater. **30**, 683 (1994).
²¹L. Wang, Z. Fan, and D. E. Laughlin, Scr. Mater. **47**, 781 (2002).
²²Y. M. Jin, Y. U. Wang, A. Kazaryan, Y. Wang, D. E. Laughlin, and A. G. Khachatryan, J. Appl. Phys. **92**, 6172 (2002).
²³W. F. Brown, Jr., *Micromagnetics* (Wiley, New York, 1963).
²⁴A concise review of various methods for calculation of magnetostatic energy can be found in D. V. Berkov, K. Ramsrock, and A. Hubert, Phys. Status Solidi A **137**, 207 (1993).
²⁵A. G. Khachatryan, *Theory of Structural Transformations in Solids* (Wiley, New York, 1983).